Supporting Information

Bio-Ingredients Assisted Formation of Porous TiO_2 for Li-Ion Battery Electrodes

*Yi-Chun Chang, Chih-Wei Peng, Po-Chin Chen, Chi-Young Lee, and Hsin-Tien Chiu**

Yi-Chun Chang, Chih-Wei Peng, Po-Chin Chen, Prof. Hsin-Tien Chiu
Department of Applied Chemistry, National Chiao Tung University, Hsinchu, Taiwan 30010, R. O. C.
Fax: (886)-3-5723764
E-mail: htchiu@nctu.edu.tw

Prof. Chi-Young Lee
Department of Materials Science and Engineering, National Tsing Hua University, Hsinchu, Taiwan 30013, R. O. C.

Figure S1. SEM image of the reference sample.

Figure S2. EDX result from the rectangular area in the TEM image of C-PT. The same image is displayed in Figure 4a in the main article also.

Figure S3. Raman spectrum of C-PT.

Figure S4. SEM image of C-PT.

Figure S5. XRD pattern of C-PT.

Figure S6. N_2 adsorption-desorption isotherms of sample C-PT. Inset: pore size distributions of the material.

Figure S7. Four continuous scans of cyclic voltammograms of (a) PT and (b) the reference sample.

Figure S8. Discharge/charge curves of anodes composed of (a) C-PT, (b) C-PT-2, (c) PT, and (d) the reference sample at 3 - 1 V versus Li^+/Li.

Figure S9. Rate capacities of C-PT at 5 C (1 C = 334 mAh/g) for 100 cycles.

Figure S10. (a) Impedance plots of the samples before cycling. (b) Plots of impedance as a function of the inversed square root of angular frequency in the Warburg region.

Figure S11. (a) Impedance plots of C-PT before and after discharge-charge cyclings. (b) Plots of impedance as a function of the inversed square root of angular frequency in the Warburg region.

Table S1. Summary of electrochemical properties of the anatase TiO_2 anode materials for Li-ion batteries. All cathodes are Li metal foils.

Table S2. Warburg factors (σ) and diffusion coefficients (D) (estimated from the equations S1 and S2 below) of Li ions in different anode samples.

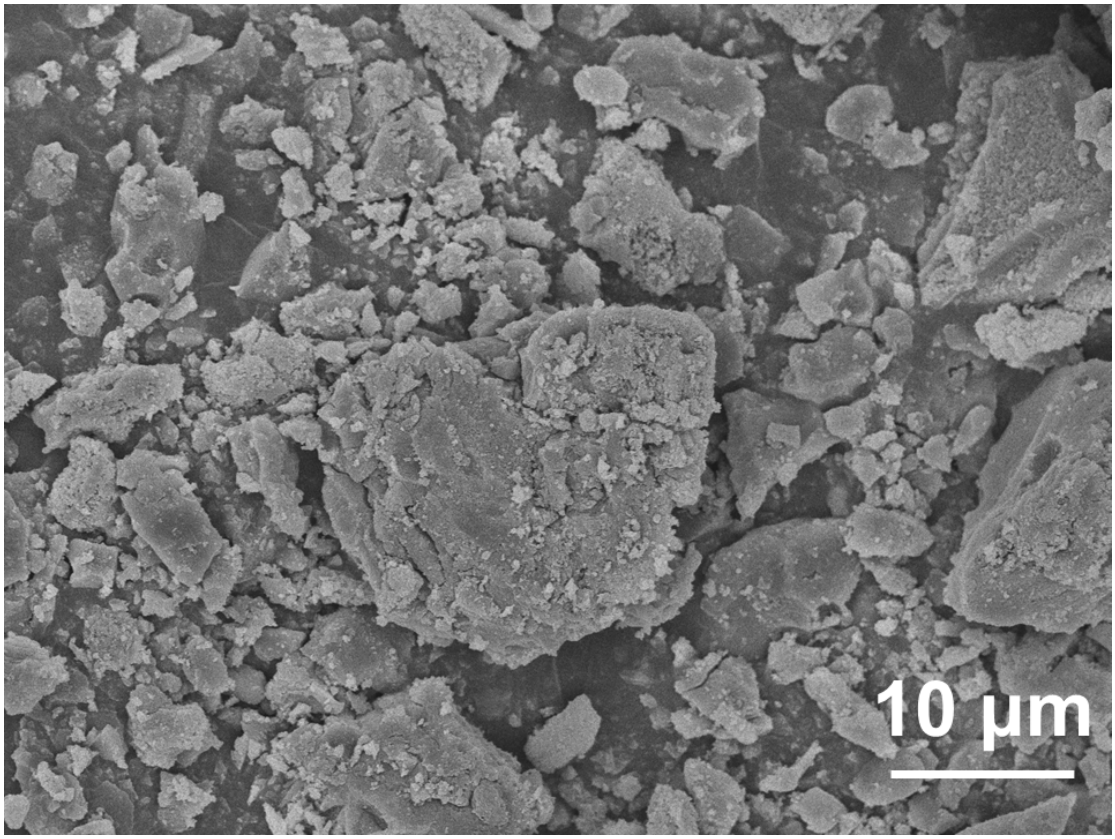

Figure S1. SEM image of the reference sample.

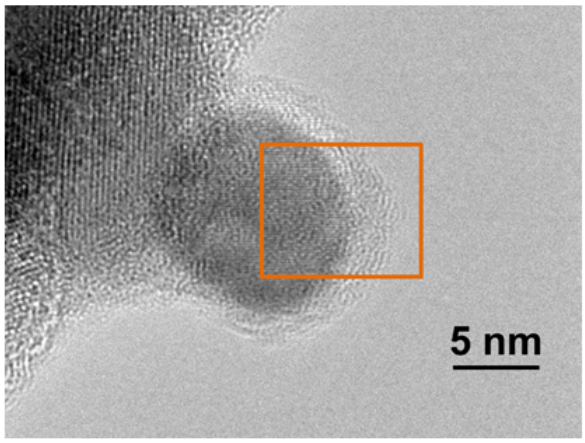

Element	Atomic %
C	56.05
O	24.03
Ti	19.91

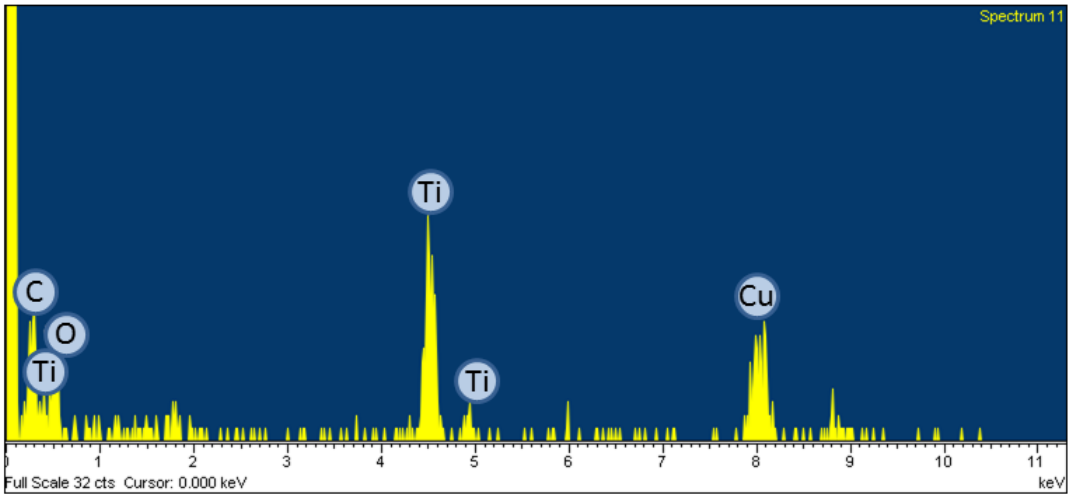

Figure S2. EDX result from the rectangular area in the TEM image of C-PT. The same image is displayed in Figure 4a in the main article also.

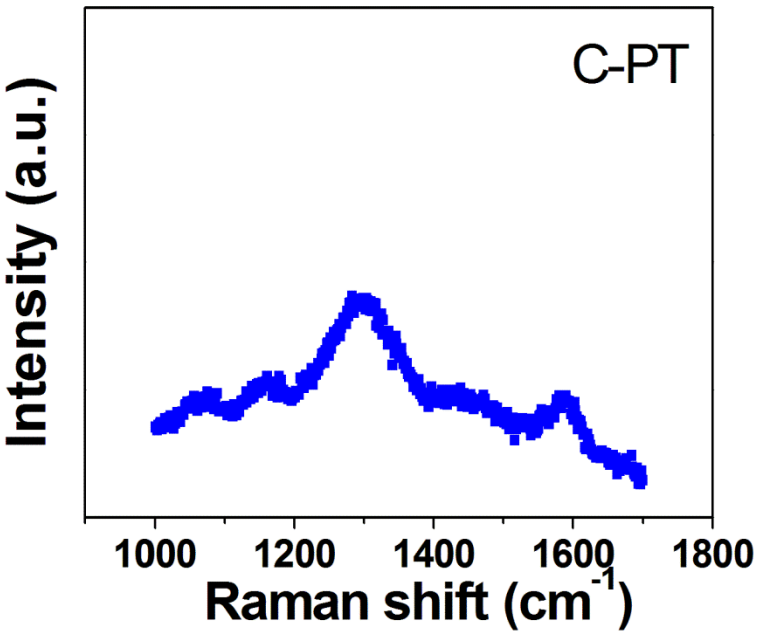

Figure S3. Raman spectrum of C-PT.

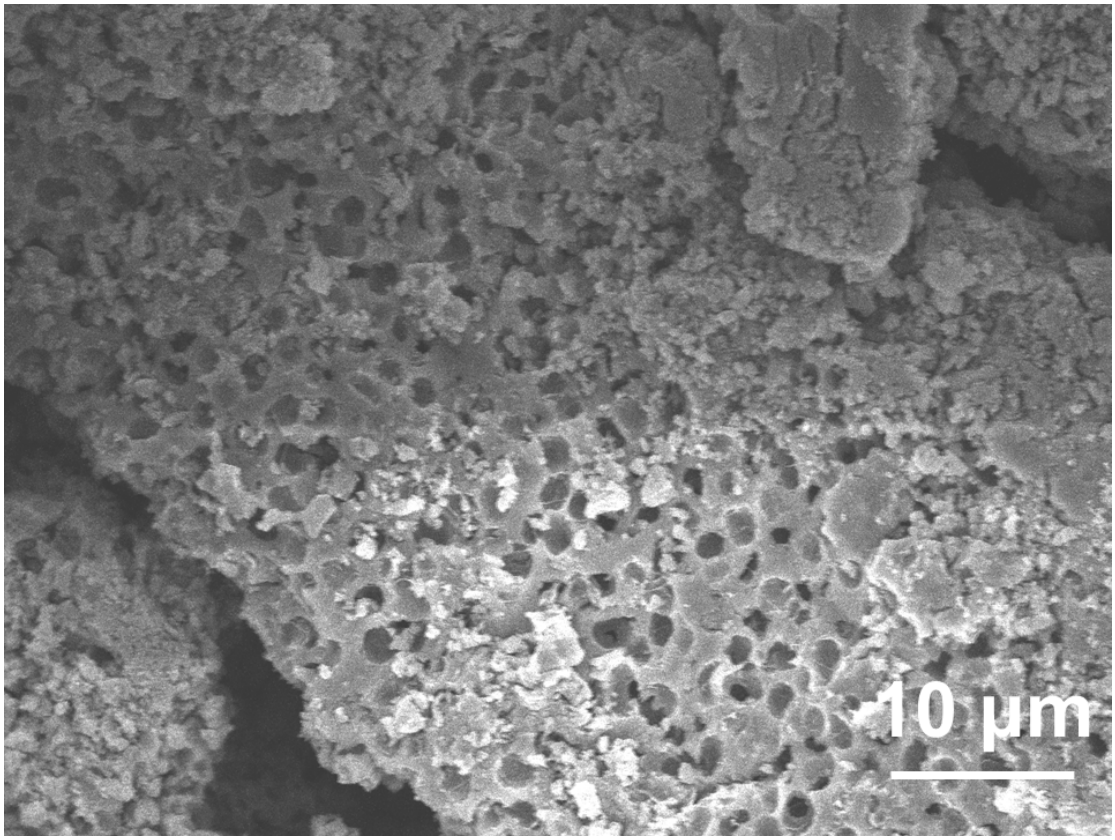

Figure S4. SEM image of C-PT.

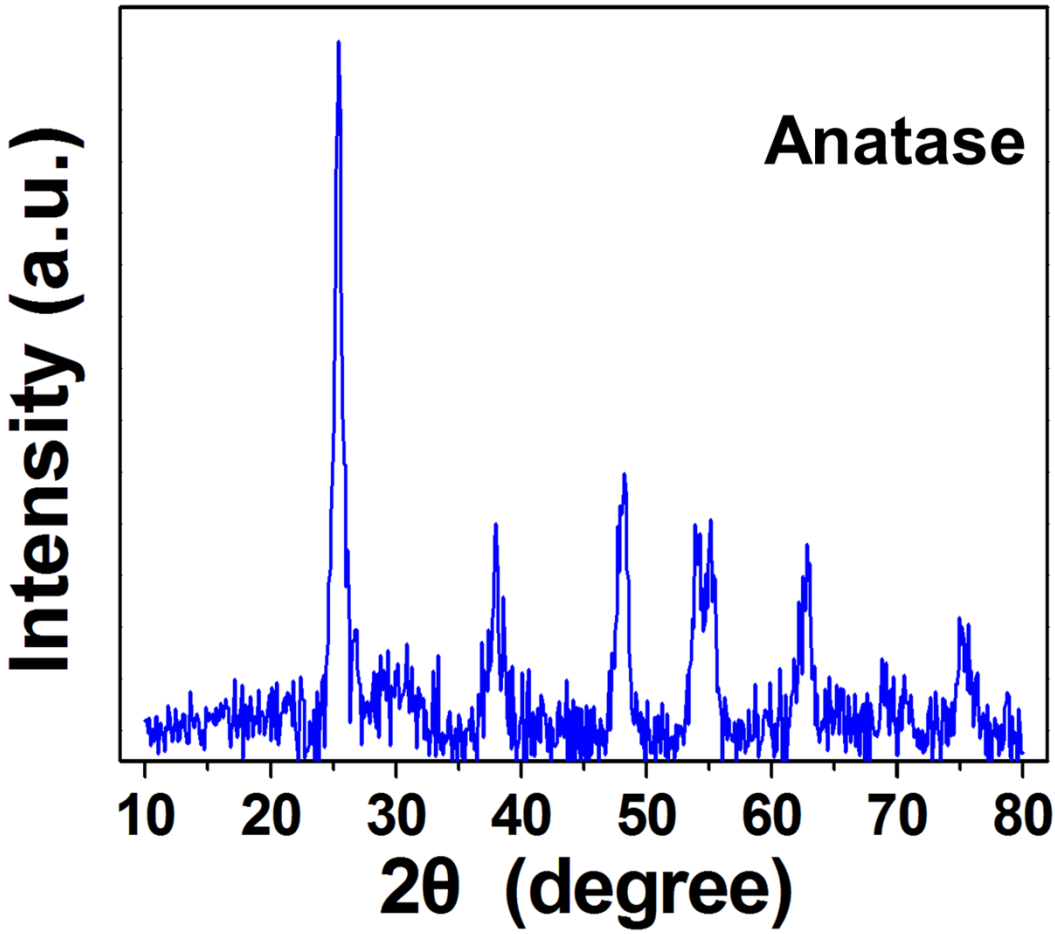

Figure S5. XRD pattern of C-PT.

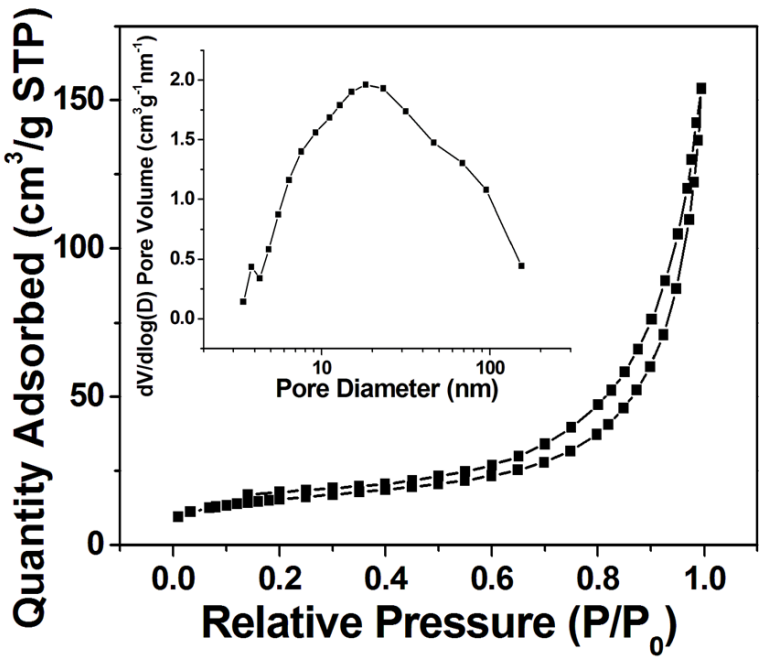

Figure S6. N_2 adsorption-desorption isotherms of sample C-PT. Inset: pore size distributions of the material.

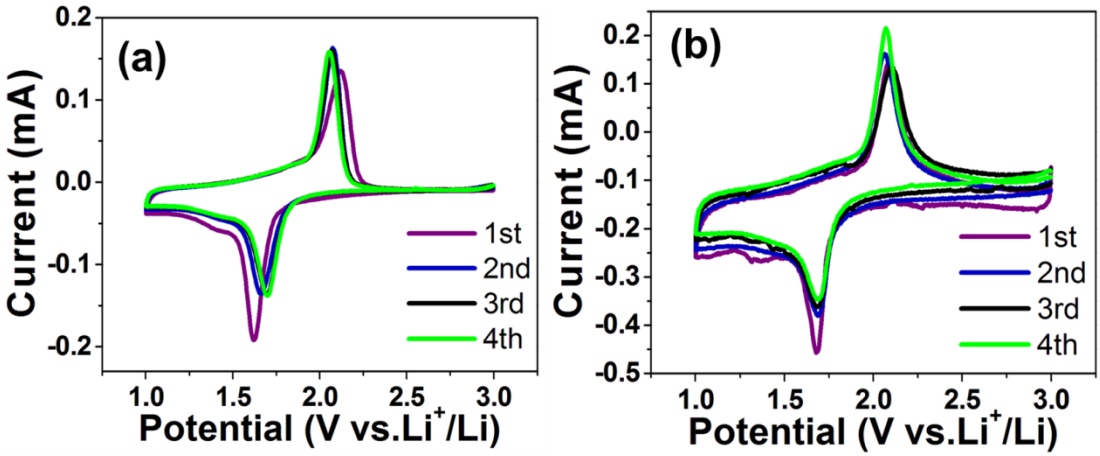

Figure S7. Four continuous scans of cyclic voltammograms of (a) PT and (b) the reference sample.

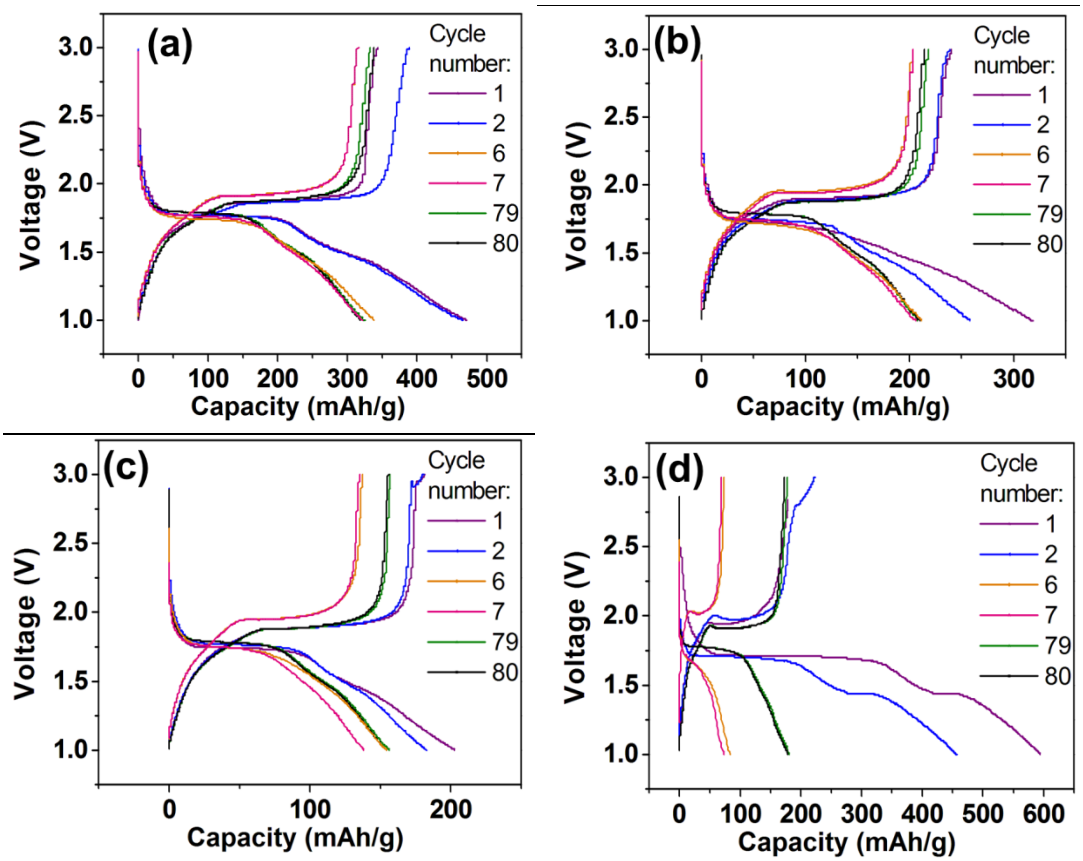

Figure S8. Discharge/charge curves of anodes composed of (a) C-PT, (b) C-PT-2, (c) PT, and (d) the reference sample at 3 - 1 V versus Li^+/Li.

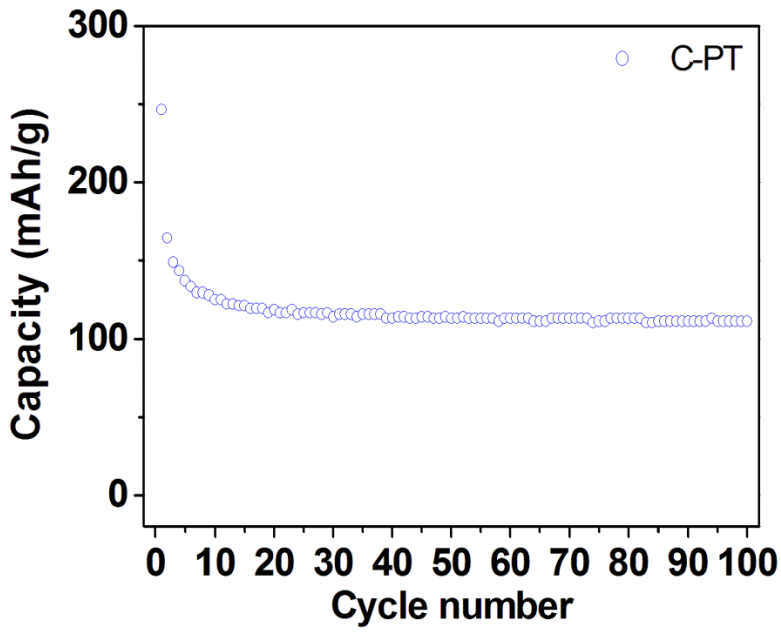

Figure S9. Rate capacities of C-PT at 5 C (1 C = 334 mAh/g) for 100 cycles.

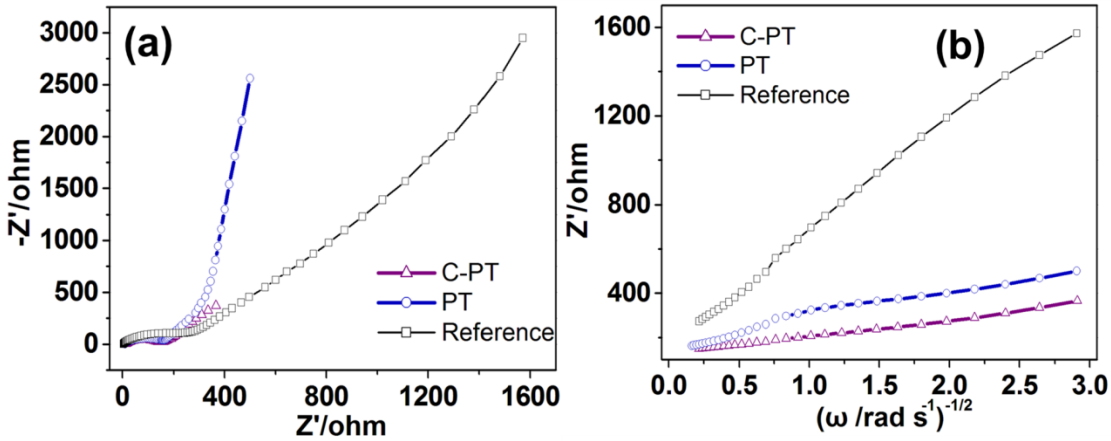

Figure S10. (a) Impedance plots of the samples before cycling. (b) Plots of impedance as a function of the inversed square root of angular frequency in the Warburg region.

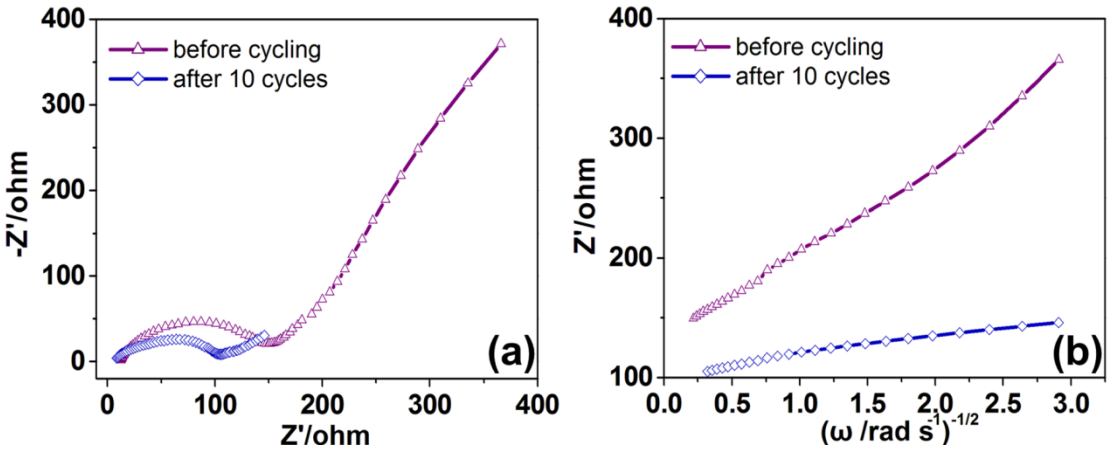

Figure S11. (a) Impedance plots of C-PT before and after discharge-charge cyclings. (b) Plots of impedance as a function of the inversed square root of angular frequency in the Warburg region.

Table S1. Summary of electrochemical properties of the anatase TiO_2 anode materials for Li-ion batteries. All cathodes are Li metal foils.

TiO_2 Anode Materials	Morphology	Surface area (m^2/g)	Performance			References
			Working Potential (V)	Cycling Rate (mA/g)	Capacity (mAh/g)	
Anatase	Nanotube	400	1.2 - 3	4000	105	58[a]
Anatase	Nanosheet	170	1 - 3	85	224	46[b]
				3400	95	
Anatase	Hollow sphere	135	1 - 3	1700	98	59[c]
Anatase	Spindle-shaped	16	1 - 3	170	152	60[d]
Anatase	Nanocage	64	1 - 3	85	140	47[e]
Anatase	Porous	70	1 - 3	2000	87	45[f]
Anatase	Micro sphere	118	1 - 3	680	176	61[g]
				1700	151	
				3400	125	
Anatase/Rutile[1]	Micro sphere	54	1 - 3	5100	103	62[h]
C/Anatase[2]	Mesoporous	120	1 - 3	170	166	18[i]
N-doped C/Anatase[3]	Nanofiber	191	1 - 3	33	264	19[j]
				1650	155	
C/Anatase[2]	Porous	53	1 - 3	1670	180	This work
				3340	142	

1. Mixed phases.
2. C-coated anatase.
3. N-doped C coated anatase.

a. Wang, K.; Wei, M.; Morris, M. A.; Zhou, H.; Holmes, J. D., Mesoporous Titania Nanotubes: Their Preparation and Application as Electrode Materials for Rechargeable Lithium Batteries. *Adv. Mater.* **2007,** *19* (19), 3016-3020.
b. Chen, J. S.; Tan, Y. L.; Li, C. M.; Cheah, Y. L.; Luan, D.; Madhavi, S.; Boey, F. Y. C.; Archer, L. A.; Lou, X. W., Constructing Hierarchical Spheres from Large Ultrathin Anatase TiO_2 Nanosheets with Nearly 100% Exposed (001) Facets for Fast Reversible Lithium Storage. *J. Am. Chem. Soc.* **2010,** *132* (17), 6124-6130.
c. Ding, S.; Chen, J. S.; Wang, Z.; Cheah, Y. L.; Madhavi, S.; Hu, X.; Lou, X. W., TiO_2 hollow spheres with large amount of exposed (001) facets for fast reversible lithium storage. *J. Mater. Chem.* **2011,** *21* (6), 1677-1680.
d. Ye, J.; Liu, W.; Cai, J.; Chen, S.; Zhao, X.; Zhou, H.; Qi, L., Nanoporous Anatase TiO_2 Mesocrystals: Additive-Free Synthesis, Remarkable Crystalline-Phase Stability, and Improved Lithium Insertion Behavior. *J. Am. Chem. Soc.* **2010,** *133* (4), 933-940.
e. Wang, Z.; Lou, X. W., TiO_2 Nanocages: Fast Synthesis, Interior Functionalization and Improved Lithium Storage Properties. *Adv. Mater.* **2012,** *24* (30), 4124-4129.
f. Zhang, D.; Wen, M.; Zhang, P.; Zhu, J.; Li, G.; Li, H., Microwave-Induced Synthesis of Porous Single-Crystal-Like TiO_2 with Excellent Lithium Storage Properties. *Langmuir* **2012,** *28* (9), 4543-4547.
g. Ma, Y.; Ji, G.; Ding, B.; Lee, J. Y., Facile solvothermal synthesis of anatase TiO_2 microspheres with adjustable mesoporosity for the reversible storage of lithium ions. *J. Mater. Chem.* **2012,** *22* (46), 24380-24385.
h. Shen, J.; Wang, H.; Zhou, Y.; Ye, N.; Li, G.; Wang, L., Anatase/rutile TiO_2 nanocomposite microspheres with hierarchically porous structures for high-performance lithium-ion batteries. *R. Soc. Chem. Adv.* **2012,** *2* (24), 9173-9178.
i. Zeng, L. X.; Zheng, C.; Xia, L. C.; Wang, Y. X.; Wei, M. D., Ordered mesoporous TiO_2-C nanocomposite as an anode material for long-term performance lithium-ion batteries. *J. Mater. Chem. A* **2013,** *1* (13), 4293-4299.
j. Ryu, M. H.; Jung, K. N.; Shin, K. H.; Han, K. S.; Yoon, S. K., High Performance N-Doped Mesoporous Carbon Decorated TiO_2 Nanofibers as Anode Materials for Lithium-Ion Batteries. *J. Phys. Chem. C* **2013,** *117* (16), 8092-8098.

Table S2. Warburg factors (σ) and diffusion coefficients (D) (estimated from the equations S1 and S2 below) of Li ions in different anode samples.

Sample	σ (ohm $cm^2/s^{0.5}$)	D (cm^2/s)
PT	125.9	$2.27*10^{-13}$
C-PT	75.233	$6.36*10^{-13}$
Reference	508.82	$1.39*10^{-13}$

Derivation of Warburg factor

$$Z_{real} = R_e + R_{ct} + \sigma\omega^{-0.5} \quad \text{(S1)}$$

Z_{real}: Real resistance of the impedance response of the system
R_e: Resistance between the electrolyte and the electrode
R_{ct}: Charge transfer resistance
σ: Warburg factor in ohm $cm^2/s^{0.5}$
ω: Angle frequency

Warburg diffusion equation

$$D = 0.5\left(\frac{RT}{AF^2\sigma C}\right)^2 \quad \text{(S2)}$$

D: Diffusion coefficient of Li^+ ions in the electrode
R: Gas constant, 8.314 J/mol K
T: Room temperature, 298 K
A: Surface area of the electrode
F: Faraday constant, 96486 C/mole
C: Molarity of Li^+ ions
σ: Warburg factor in ohm $cm^2/s^{0.5}$